Nanoscale

RSC Publishing

PAPER

View Article Online
View Journal | View Issue

Cite this: *Nanoscale*, 2013, **5**, 11003

Analytical analysis of the generic SET and RESET characteristics of electrochemical metallization memory cells

Stephan Menzel*[a] and Rainer Waser[ab]

Received 2nd July 2013
Accepted 26th August 2013

DOI: 10.1039/c3nr03387b

www.rsc.org/nanoscale

We report on an analytical model which describes the bipolar resistive switching in electrochemical metallization cells. To simulate the resistive switching, we modeled the growth and dissolution of a metallic filament together with electron tunneling between the growing filament and the counter electrode. The model accounts for the controllability of the low resistive state and the RESET current by tuning the SET current. By analytical analysis the relevant conditions for these generic characteristics are identified. In addition, an explanation for the asymmetry in the SET and RESET switching characteristics is presented. The results of the analytical analysis is generalized to all types of ReRAMs.

Introduction

Resistively switching materials have attracted great attention due to their potential application as Resistive Random Access Memory (ReRAM) in future nonvolatile memories.[1–3] Thereby, the digital information is encoded as different resistance states which can be programmed by applying appropriate electrical stimuli. Typically, ReRAM cells consist of a simple metal/insulator/metal structure, where the insulating layer is a mixed ionic–electronic conductor. During the SET operation the ReRAM cell is switched from a high resistive state (HRS) to a low resistive state (LRS), whereas during RESET the HRS is restored. Based on the intrinsic switching mechanism three different types of ReRAMs can be identified: electrochemical memory (ECM), valence change memory (VCM) and thermochemical memory (TCM). While the ECM- and VCM-type resistive memories show a bipolar operation scheme, *i.e.* different voltage polarities are required to switch between different resistance states; thermochemical memories operate at one voltage polarity. The switching mechanism in ECM cells relies on the electrochemical growth and dissolution of a copper or silver filament within the insulating layer.[4] ECM cells typically consist of an active silver or copper electrode, an ion conducting switching layer and an inert counter electrode. By applying a positive potential to the active electrode silver/copper is oxidized. The corresponding cations migrate towards the counter electrode. A reduction occurs at the counter electrode and a silver/copper filament subsequently grows towards the active electrode. As soon as an electronic contact is achieved, *e.g.* by the onset of electron tunneling between the filament and the active electrode, the resistance drops to the LRS.[5] To RESET the cell the voltage polarity is reversed and the filament dissolves. In contrast, the resistive switching in VCM cells is attributed to the migration of oxygen vacancies within the applied electric field and a subsequent change in the electronic conductivity, *e.g.* by modulation of the barrier height of one metal–insulator interface.[3] In thermochemical memories high thermal gradients play the dominant role within the switching process, which leads to a unipolar operation.[6]

Independent of the intrinsic switching mechanism ReRAMs show some generic SET and RESET switching characteristics.[5,7] The LRS can be tuned over many orders of magnitude by limiting the current I_{SET} during the SET operation to different levels, *i.e.* $R_{LRS} \propto {I_{SET}}^{-1}$. On the other hand the RESET current depends linearly on the SET current: $I_{RESET} \propto I_{SET}$. These generic switching characteristics have been first observed in ECM cells[8–10] using a simple current compliance.[11,12] Typically, the *I–V* characteristics show an asymmetry, *i.e.* the RESET current is lower than the SET current. Recently, this behavior has also been demonstrated for VCM and TCM systems.[13] In the latter study the multilevel switching has been attributed to a variation of the filament diameter. The RESET has been described as thermally activated dissolution of the filament, which was shown to yield in the experimental correlation between SET and RESET current. Here, SET and RESET currents are almost equal. While this model seems to be applicable for low resistive LRS states, it fails for high resistive LRS. In this case the typical RESET currents can be less than a few μA at a typical RESET voltage in ECM cells below 0.5 V. Thus, a significant temperature increase is not expected in this regime. Instead of a diameter variation we proposed the modulation of a tunneling gap between the growing metallic filament and an

[a]*Peter Grünberg Institut, Forschungszentrum Jülich GmbH, Jülich, 52425, Germany. E-mail: t.menzel@fz-juelich.de*

[b]*Institut für Werkstoffe der Elektrotechnik II, RWTH Aachen University, Aachen, 52074, Germany*

active electrode as the origin of the multilevel switching in ECM cells in this regime.[5] In fact, experimental results indicate that a transition between the variable gap and the variable diameter model occurs in ECM cells at the resistance of a single-atom contact, which is about 12.9 kΩ.[14] At and below this value quantized conduction steps have been observed in ECM cells.[10,15] In addition, at this resistance value a change in the resistance drift behavior of ECM cells has been observed.[16] Furthermore, a transition between pure bipolar and unipolar device operation is reported for this resistance regime.[17–20] The pure bipolar operation can be related to the tunneling gap mode. The unipolar operation can be explained in the presence of a galvanic contact (*i.e.* variable diameter mode) as a thermally-assisted self-dissolution of the metal filament.[20] A transition between the variable gap and the variable width case has also been recently proposed for hafnium oxide based VCM cells.[21] It should be noted that the large range of programmable LRS resistances has been extracted from dynamic *I–V* measurements. However, in a stationary state a tunnelling gap as well as an atomic scale filament might be relatively unstable.[22] Non-equlibrium states in this configuration such as electromotive force, chemical potential gradients, size effects or electrolyte non-stoichiometry could be a reason for this instability.[23]

The first simulation models for ECM cells were presented by Russo *et al.* using a variable diameter model[24] and Menzel *et al.* for a vertical filament growth limited by electron transfer reactions[25] both in 2009. Later, Yu *et al.* proposed a model combining vertical and radial growth.[26] Recently, we presented a physical compact model for multilevel switching in ECM cells based on a variable tunneling gap.[5] In the present paper an analytical model for the high resistive LRS regime based on our previous numerical variable gap model is derived. Using this analytical model the relevant physical conditions for the generic SET and RESET characteristics in this regime are discussed. By comparing the results of this study to the variable diameter case for low resistive LRS more of these results can be generalized.

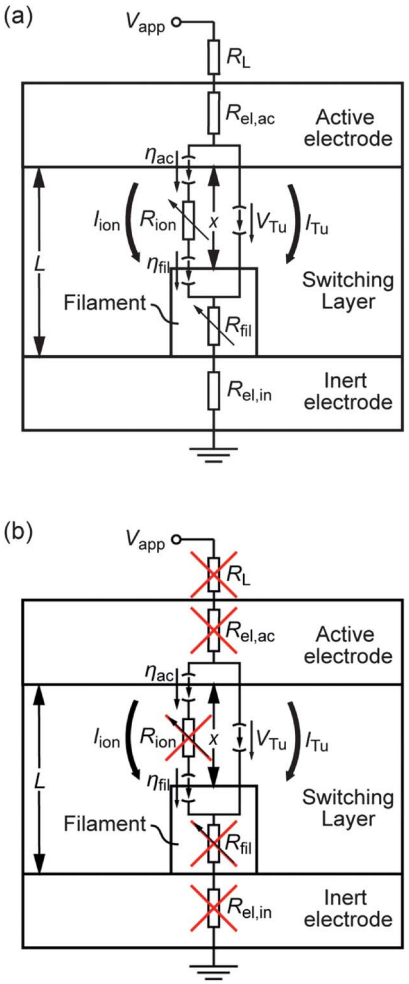

Fig. 1 Equivalent circuit diagram of the (a) numerical model[5] and (b) the simplified analytical model. The crossed-out elements are neglected in the simplified model.

ECM model

Physical compact model

Fig. 1(a) shows the equivalent circuit diagram describing the numerical variable gap model. The switching layer of thickness L is sandwiched between an active top and an inert bottom electrode. Within the switching layer a cylindrical filament with area A_{fil} is considered, which grows/dissolves when a voltage V_{app} is applied. Consequently, the tunnelling gap x between the filament tip and the active electrode is modulated. Hence, the filament resistance R_{fil} and the ionic drift resistance R_{ion} are a function of the tunnelling gap. In a more microscopic picture, the filament will have some curvature, and the deposition/dissolution of a single metal ion can take place at the very top as well as the sides of the filament. This could also lead to the occurrence of discrete current jumps. In our model the filament radius and the tunneling gap are regarded as effective parameters, which allows for continuous values.

In the present study we consider only the variable gap regime, *i.e.* LRS resistances higher than 12.9 kΩ. Furthermore, we restrict our maximum current to approximately 20 μA. In this case the dissipated power is also lower than 20 μW and thus a significant Joule heating can be excluded.[27,28] Note that the active electrode as well as the filament consists of Cu or Ag, which are very good heat conductors enabling fast heat dissipation. Thus, a constant temperature of $T = 300$ K is assumed. At higher current levels and power Joule heating might affect the switching currents and needs to be considered in the model.

In the model the filamentary dissolution/growth and thus the change of the tunneling gap x is modeled by Faraday's law:[29,30]

$$\frac{dx}{dt} = -\frac{M_{Me}}{ze\rho_{m,Me}} J_{Me^{z+}}, \quad (1)$$

where $J_{Me^{z+}}$ is the ionic current density, z the charge transfer number, M_{Me} the atomic mass and $\rho_{m,Me}$ the mass density of the deposited metal. The ionic current is limited by the electron transfer reaction occurring at the metal/insulator boundaries. The associated current density is described by the Butler–Volmer equation[30]

$$J_{Me^{z+}} = J_{BV}(\eta) = j_0\left\{\exp\left(\frac{(1-\alpha)ez}{kT}\eta\right) - \exp\left(-\frac{\alpha ez}{kT}\eta\right)\right\}, \quad (2)$$

which depends on the electron transfer overpotential η. In eqn (2) j_0 denotes the exchange current density and α the charge transfer coefficient. If η is positive the first term describing the oxidation process dominates, whereas the second term overweighs for negative η. Since the ionic current depends exponentially on the overpotential, the switching process exhibits a nonlinear switching kinetics. For an intermediate voltage range the tunneling current I_{Tu} between the growing filament and the active electrode can be calculated according to Simmons[31] as a nonlinear function of the controlling voltage V_{Tu} to

$$I_{Tu} = \frac{eA_{fil}}{2\pi hx^2}\left(\Delta W_0 - \frac{eV_{Tu}}{2}\right)\exp\left(-\frac{4\pi x}{h}\sqrt{2m_{eff}}\sqrt{\Delta W_0 - \frac{eV_{Tu}}{2}}\right) - \frac{eA_{fil}}{2\pi hx^2}\left(\Delta W_0 + \frac{eV_{Tu}}{2}\right)\exp\left(-\frac{4\pi x}{h}\sqrt{2m_{eff}}\sqrt{\Delta W_0 + \frac{eV_{Tu}}{2}}\right) \quad (3)$$

here, ΔW_0 is the tunneling barrier height, $m_{eff} = m_r m_0$ the electron effective mass of the insulating material, A_{fil} the filament area and h Planck's constant. Since the tunneling current depends exponentially on the tunneling gap x, a wide range of resistance states can be achieved by controlling the gap. Fig. 1 shows the equivalent circuit diagram of the simulation model. The overpotentials at the filament–insulator interface and the active electrode–insulator interface are denoted as η_{fil} and η_{ac}, respectively. Using Kirchhoff's laws an implicit equation for the filamentary overpotential η_{fil} can be obtained for an applied voltage or imposed current.[5] Thus, the differential equation (1) can be solved numerically. This model has been extended recently to also cover nucleation effects and nonlinear ion hopping transport.[32] Note that the derived model is inherently dynamic and covers the dynamic switching behaviour when a voltage is applied. It does not give information about the long-term stability of different programmed resistance states.

Simplified model

To obtain an analytical model for ECM switching the physical compact model needs to be simplified. Especially, it is necessary to eliminate the implicit equations for the overpotential η_{fil} and for the tunneling voltage V_{Tu} (*cf.* eqn (3)). According to our previous simulations the voltage drops across the electrodes given by $I_{cell}R_{el}$ and the ionic conductor $V_{ion} = I_{ion}R_{ion}$ are small compared to the overpotentials η_{fil} and η_{ac}.[5] Furthermore, the nonlinear hopping is not relevant in the electron transfer regime.[32] Thus, the overall cell voltage can be simplified to $V_{cell} \approx V_{Tu} \approx \eta_{ac} - \eta_{fil}$. This simplification is valid as long as a moderate current compliance $I_{cc} \leq 10$ μA is chosen and the load resistor is negligible. The resulting equivalent circuit diagram is shown in Fig. 1(b). According to eqn (3) V_{Tu} can only be obtained numerically if the gap x and the current I_{Tu} are known. Since ECM cells exhibit an ohmic *I–V* characteristic in the ON state, a linear relationship between the tunneling current and the voltage according to Simmons[31] is applicable:

$$I_{Tu} = C\frac{3\sqrt{2m_{eff}\Delta W_0}}{2x}\left(\frac{e}{h}\right)^2\exp\left(-\frac{4\pi x}{h}\sqrt{2m_{eff}\Delta W_0}\right)A_{fil}V_{Tu} = G_{Tu}(x)V_{Tu} \quad (4)$$

In contrast to the equation derived by Simmons[31] an additional factor C is introduced in eqn (4). The value of C is optimized by a least squares method such that the *I–V* relationships of eqn (3) and (4) coincide for the set of parameters used in this study, which results in $C = 0.29$. Eqn (4) can now be solved for x using the Lambert-*W* function $W(\cdot)$ that gives the solution of the equation $xe^x = a$ as $x = W(a)$.[33] Rewriting eqn (4) and applying the Lambert-*W* function yields

$$x = \frac{h}{4\pi\sqrt{2m_{eff}\Delta W_0}}W\left(C\frac{12m_{eff}\pi\Delta W_0 e^2 A_{fil}V_{Tu}}{h^3 I_{Tu}}\right) \quad (5)$$

In this case the electronic tunneling current can be directly calculated if the cell voltage V_{cell}, which equals V_{Tu}, and the gap x are known.

To eliminate the implicit equations for the overpotential η_{fil} the following simplification applies: for overpotentials $|\eta| \gg k_BT/ze$ one of the two terms in eqn (2) can be neglected. So for the SET operation the ionic current at the active electrode–insulator interface $I_{ac,SET}$ is

$$I_{ac,SET}(\eta_{ac,SET}) = j_0 A_{ac}\exp\left(\frac{(1-\alpha)ez}{kT}\eta_{ac,SET}\right), \quad (6)$$

and at the filament–insulator interface

$$I_{fil,SET}(\eta_{fil,SET}) = j_0 A_{fil}\exp\left(-\frac{\alpha ez}{kT}\eta_{fil,SET}\right) \quad (7)$$

holds. Note that ECM cells are mixed ionic electronic conductors and the ionic conduction could dominate in the HRS, *e.g.* in Cu/SiO2/Pt cells.[34] In the latter case the ionic currents define the resistance state as long as parallel electronic leakage currents are neglected. Due to charge neutrality these two ionic currents have to be equal and thus $\eta_{ac,SET}$ can be expressed as a function of $\eta_{fil,SET}$ by

$$\eta_{ac,SET} = -\frac{\alpha}{1-\alpha}\eta_{fil,SET} + \frac{k_BT}{ze(1-\alpha)}\ln\left(\frac{A_{fil}}{A_{ac}}\right). \quad (8)$$

Inserting eqn (8) into $V_{cell,SET} \approx \eta_{ac,SET} - \eta_{fil,SET}$ gives

$$\eta_{fil,SET} = -(1-\alpha)V_{cell} + \frac{k_BT}{ze}\ln\left(\frac{A_{fil}}{A_{ac}}\right). \quad (9)$$

The ordinary differential equation (1) can now be rewritten using eqn (7) and (9) to

$$\frac{dx}{dt} = -\frac{M_{Me}}{ze\rho_{m,Me}}j_0\left(\frac{A_{ac}}{A_{fil}}\right)^{\alpha}\exp\left(\alpha(1-\alpha)\frac{ze}{k_BT}V_{cell}(t)\right), \quad (10)$$

which describes the filamentary growth during the voltage-controlled SET operation. During current control the cell voltage is replaced using eqn (4) by $V_{cell} = I_{cc}(t)/G_{Tu}(x)$.

Similarly, an expression for the filamentary overpotential during RESET operation can be found:

$$\eta_{fil,RESET} = -\alpha V_{cell} - \frac{k_BT}{ze}\ln\left(\frac{A_{fil}}{A_{ac}}\right). \quad (11)$$

Equivalently, it yields

$$\frac{\mathrm{d}x}{\mathrm{d}t} = \frac{M_{\mathrm{Me}}}{ze\rho_{\mathrm{m,Me}}} j_0 \left(\frac{A_{\mathrm{ac}}}{A_{\mathrm{fil}}}\right)^{1-\alpha} \exp\left(-\alpha(1-\alpha)\frac{ze}{k_{\mathrm{B}}T} V_{\mathrm{cell}}(t)\right) \quad (12)$$

for the voltage-controlled RESET operation. Note that the cell voltage is negative during the RESET operation. The ordinary differential equations (10) and (12) can be solved analytically for some special cases under voltage control. During the current control eqn (10) still needs to be solved numerically since no analytical solution exists.

Analytical solution of the simplified model

In experiments a triangular voltage sweep with a set current compliance is commonly used. For this case the differential equations (11) and (12) are solved analytically as discussed in the following. Due to the shape of the voltage signal the time-dependent cell voltage is defined piecewise. As a simplification it is assumed that the current compliance is reached before the peak voltage V_{p} is reached, *i.e.* $t_{\mathrm{SET}} < t_{\mathrm{rise}}$. The cell voltage in this regime is $V_{\mathrm{cell}} = V_{\mathrm{p}}/t_{\mathrm{rise}} t = \beta t$ with sweep rate β. Partial integration of eqn (10) yields

$$x = L - \frac{M_{\mathrm{Me}}}{ze\rho_{\mathrm{m,Me}}} j_0 \left(\frac{A_{\mathrm{ac}}}{A_{\mathrm{fil}}}\right)^{\alpha} \frac{k_{\mathrm{B}}T}{\alpha(1-\alpha)ze\beta} \times \left(\exp\left(\alpha(1-\alpha)\frac{ze}{k_{\mathrm{B}}T}\beta t\right) - 1\right) \quad (13)$$

as the solution for the gap x. It is valid until the current compliance is reached. This upper boundary is determined as follows: when the current compliance value I_{SET} is reached the gap is calculated by

$$x_{\mathrm{SET}} = L - \frac{M_{\mathrm{Me}}}{ze\rho_{\mathrm{m,Me}}} j_0 \left(\frac{A_{\mathrm{ac}}}{A_{\mathrm{fil}}}\right)^{\alpha} \frac{k_{\mathrm{B}}T}{\alpha(1-\alpha)ze\beta} \exp\left(\alpha(1-\alpha)\frac{ze}{k_{\mathrm{B}}T} V_{\mathrm{SET}}\right). \quad (14)$$

The SET voltage in eqn (14) can be replaced according to eqn (5) with

$$V_{\mathrm{SET}} = \frac{2h^2}{3Ce^2\sqrt{2m_{\mathrm{eff}}\Delta W_0}} x_{\mathrm{SET}} \exp\left(\frac{4\pi}{h} x_{\mathrm{SET}}\sqrt{2m_{\mathrm{eff}}\Delta W_0}\right) \frac{I_{\mathrm{SET}}}{A_{\mathrm{fil}}} \quad (15)$$

since the LRS resistance is given by the linear tunnel equation (*cf.* eqn (4)). Now eqn (14) can be solved for x_{SET} numerically, which in turn gives the upper boundary for V_{SET} and t_{SET}, respectively.

For the RESET process starting at $t = T_0 = 2t_{\mathrm{rise}}$ the integration has to be conducted separately for $T_0 < t \leq T_0 + t_{\mathrm{rise}}$ and $T_0 + t_{\mathrm{rise}} < t \leq 2T_0$, respectively. In the former time period the cell voltage reads $V_{\mathrm{cell}}(t) = -V_{\mathrm{p}}/t_{\mathrm{rise}}(t - T_0) = -\beta(t - T_0)$. Partial integration of eqn (12) and solving for x gives

$$x = x_{\mathrm{ON}} + \frac{M_{\mathrm{Me}}}{ze\rho_{\mathrm{m,Me}}} j_0 \left(\frac{A_{\mathrm{ac}}}{A_{\mathrm{fil}}}\right)^{1-\alpha} \frac{k_{\mathrm{B}}T}{\alpha(1-\alpha)ze\beta} \times \left(\exp\left(\alpha(1-\alpha)\frac{ze}{k_{\mathrm{B}}T}\beta(t - T_0)\right) - 1\right), \quad (16)$$

where $x_{\mathrm{ON}} = x(t = T_0)$ denotes the remaining tunneling gap after the SET process. For $T_0 + t_{\mathrm{rise}} < t \leq 2T_0$ the cell voltage is $V_{\mathrm{cell}}(t) = -2V_{\mathrm{p}} + V_{\mathrm{p}}/t_{\mathrm{rise}}(t - T_0) = \beta(t - T_0 - 2t_{\mathrm{rise}})$. Partial integration of eqn (12) with the initial value $x_{T+t_{\mathrm{rise}}}$ according to eqn (16) results in

$$x = x_{T+t_{\mathrm{rise}}} + \frac{M_{\mathrm{Me}}}{ze\rho_{\mathrm{m,Me}}} j_0 \left(\frac{A_{\mathrm{ac}}}{A_{\mathrm{fil}}}\right)^{1-\alpha} \frac{k_{\mathrm{B}}T}{\alpha(1-\alpha)ze\beta} \times \left[\exp\left(\alpha(1-\alpha)\frac{ze}{k_{\mathrm{B}}T}\beta(2t_{\mathrm{rise}} + T_0 - t)\right) - \exp\left(\alpha(1-\alpha)\frac{ze}{k_{\mathrm{B}}T} V_{\mathrm{p}}\right)\right]. \quad (17)$$

The complete *I–V* characteristic of an ECM cell can now be calculated using the analytical equations (14), (16) and (17) and during current control eqn (10) is solved numerically using an advanced Euler method until the end of the SET sweep, *i.e.* $t = T_0$. For all calculations the parameter set in Table 1 is used.

Table 1 Simulation model parameters

Symbol	Value
M_{Me}	1.06×10^{-22} g
z	2
$\rho_{\mathrm{m,Me}}$	8.95 g cm^{-3}
m_{r}	0.86
ΔW_0	4.2 eV
α	0.5
j_0	1×10^{-2} A m^{-2}
ρ_{ion}	1×10^{-2} Ω m
A_{ac}	201 nm^2
A_{fil}	201 nm^2
A_{is}	201 nm^2
L	20 nm
ρ_{fil}	2×10^{-8} Ω m
R_{el}	76.4 mΩ
R_{L}	0 Ω
T	300 K

Results

I–V characteristics

To validate the derived analytical model an *I–V* characteristic is calculated and compared to a numerical solution using our previous 1D numerical model.[5] As excitation a triangular voltage pulse with a peak voltage of $V_{\mathrm{p}} = 1$ V and a rise time $t_{\mathrm{rise}} = 1$ s is used. Fig. 2 shows the resulting *I–V* and *R–V* characteristics. Evidently, the numerical and the analytical solutions coincide. The slight difference in the *R–V* characteristics in the low voltage range of the HRS is caused by the used simplification of the Butler–Volmer equation (*cf.* eqn (6) and (7)). Since the growth speed is very low in this low voltage regime, the deviation from the numerical model is negligible. But, if a low voltage is applied for a long time with respect to the growth speed, an error occurs. The simulations show that the LRS obeys a linear *I–V* relationship according to eqn (4) and the HRS is governed by the nonlinear ionic current (*cf.* eqn (6) and (7)). Note that parallel leakage currents are not included in this model. But since these are not supposed to affect the switching, they would simply add to the total current. For further analyses we refer to the quantities SET voltage V_{SET}, ON voltage V_{ON}, SET current I_{SET}, RESET current I_{RESET} and the RESET voltage V_{RESET} as defined in Fig. 2(a).

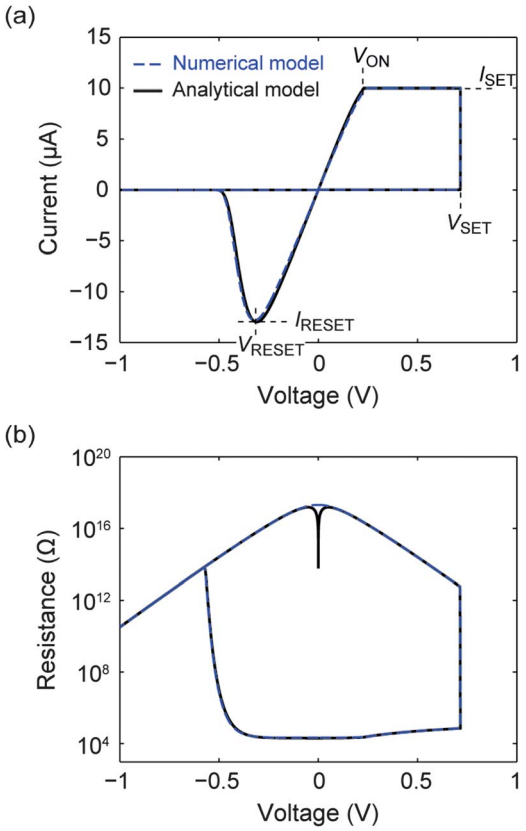

Fig. 2 Simulated (a) *I–V* characteristics, (b) *R–V* characteristics using the numerical model (blue dashed line) and the analytical model (black solid line).

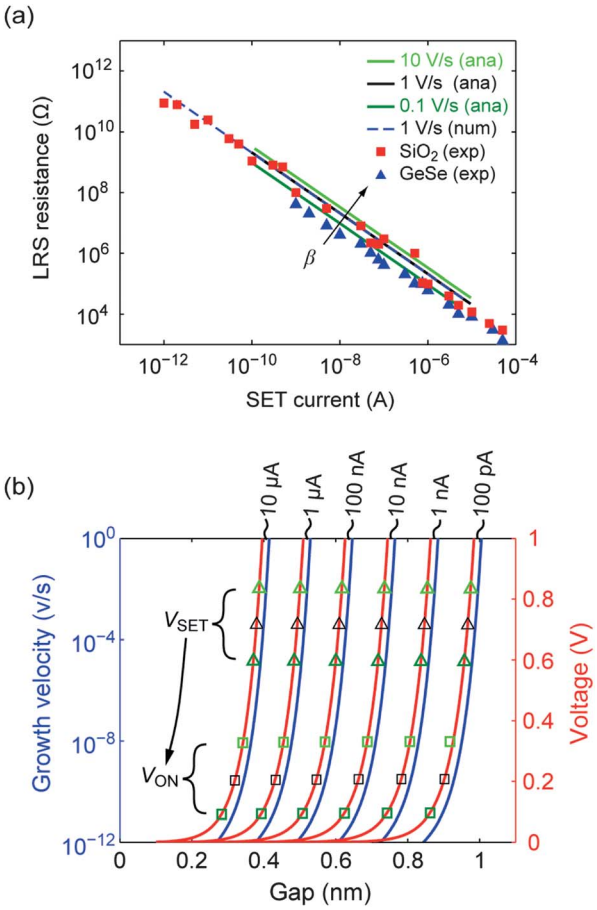

Fig. 3 (a) Calculated LRS resistance *vs.* SET current using the analytical model for sweep rates $\beta = 0.1$ V s^{-1} (dark green), 1 V s^{-1} (black), and 10 V s^{-1} (light green). For comparison the experimental data for a Cu/SiO_2 based ECM cell and a Ag/GeSe based ECM cell are shown as red squares and blue triangles, respectively. Here, only a subset of the experimental data comparable to the simulation range is shown.[9] The simulation result obtained using the numerical model[5] is illustrated as a dashed blue line. (b) Voltage (red) and growth velocity *vs.* gap under current control for different current compliances. In addition, the SET voltages V_{SET} (triangles) and ON voltages V_{ON} (squares) are shown for different sweep rates using the same color code as in (a).

In the present case the RESET current is higher than the SET current. In experiments, however, the RESET current in ECM cells is typically lower than the SET current. This asymmetry can be explained by the asymmetry of the governing differential equations (10) and (12) for SET and RESET, respectively. If the charge transfer coefficient $\alpha \neq 0.5$ and $A_{fil} \neq A_{ac}$, SET and RESET velocities differ for a certain voltage. As a consequence, the I_{SET}/I_{RESET} ratio changes.

Generic SET and RESET characteristics

To study the generic SET and RESET switching properties the *I–V* characteristics of the ECM cell are calculated using the analytical model for varying SET currents from 100 pA to 10 μA at different sweep rates $\beta = V_p/t_{rise}$. The peak voltage is 1 V in all calculations. From the calculation results the quantities V_{SET}, V_{ON}, I_{SET}, I_{RESET} and V_{RESET} are extracted and analyzed. To show the validity of the derived analytical model the calculation results are compared to previous numerical simulation results[5] and experimental data for Cu:SiO_2 and Ag:GeSe cells.[9] The set of simulation parameters used in the present analytical study (*cf.* Table 1) is identical to the one used in our previous simulations[5] in which the sweep rate was always 1 V s^{-1}.

SET

Fig. 3(a) shows the calculated LRS resistance against the SET current for different chosen sweep rates β. As a comparison data obtained from the numerical analysis[5] are depicted as a blue dashed line and the experimental data for Cu:SiO_2 cells and Ag:GeSe cells as red squares and blue triangles, respectively. The calculated behavior coincides with the simulation results of the numerical study and reproduces the experimental data very well. Evidently, the LRS resistance obeys the empirical law $R_{LRS} = V_{ON}/I_{SET}$, whereas V_{ON} depends on the sweep rate. The higher the sweep rate the higher the LRS resistance and in turn the ON voltage is also increased. To understand the controllability of the LRS the growth velocity during current control $v = dx/dt$, *i.e.* eqn (10) with V replaced using eqn (4), is analyzed in more detail. In Fig. 3(b) it is plotted against the tunneling gap x for different SET currents along with the corresponding voltage. Apparently, the v–x as well as the V–x characteristics for different SET currents are shifted parallel to each other by a constant gap. The growth velocity decreases several orders of magnitude when the gap is reduced by a small amount due to the highly nonlinear switching kinetics. Note that a growth

velocity of 0.2 nm s^{-1} is so low that the growth cannot be considered as continuous. The growth has to be rather described by the deposition of individual atoms. Thus, the growth will get statistical in this regime. The calculated SET voltages and ON voltages are marked in Fig. 3(b) for different sweep rates. For a particular sweep rate the SET voltages are virtually identical for different SET currents. At the onset of the current compliance also the growth velocities are thus virtually identical. As a consequence, an almost identical transient behavior under current control with virtually identical ON voltages results. The influence of the sweep rates on the SET voltages as well as the ON voltages increases. This correlation can be explained mathematically by rewriting eqn (14) to

$$V_{\mathrm{SET}} = \frac{k_{\mathrm{B}}T}{\alpha(1-\alpha)ze}\ln\left(\frac{(L-x_{\mathrm{SET}})z^2e^2\rho_{\mathrm{m,Me}}\alpha(1-\alpha){A_{\mathrm{fil}}}^{\alpha}}{M_{\mathrm{Me}}j_0k_{\mathrm{B}}T{A_{\mathrm{ac}}}^{\alpha}}\beta\right) \quad (18)$$

Since $L \gg x_{\mathrm{SET}}$, $L - x_{\mathrm{SET}}$ is almost constant and for the SET voltage $V_{\mathrm{SET}} \propto \ln(—)$ holds. The voltage drop during current control is $V_{\mathrm{SET}} - V_{\mathrm{ON}} \approx 0.5$ V for all sweep rates. It is related to the kinetics under current control and thus a system inherent quantity. Therefore, the SET voltage can be used as a measure of LRS resistance, which in consequence depends on the sweep rate as illustrated in Fig. 3(a). In summary, the origin of the empirical law $R_{\mathrm{LRS}} = V_{\mathrm{ON}}/I_{\mathrm{SET}}$ is related to the highly nonlinear SET switching kinetics of the ECM cell. If the voltage drops, the growth velocity is reduced exponentially. In addition, the tunneling voltage depends exponentially on the tunneling gap (*cf.* eqn (4)) and hence the growth velocity depends double-exponentially on the tunneling gap. This explains the good controllability of the LRS resistance using a current compliance. The different LRS correspond to different remaining tunneling gaps. The empirical SET law could also be explained for low resistive LRS ($R_{\mathrm{LRS}} < 12.9$ kΩ) assuming a lateral filament growth model, in which the origins of nonlinear switching kinetics from a local temperature increase.[13] If the current compliance is reached, the dissipated power and in turn the temperature is decreased. Thus, further lateral growth is suppressed. Thus, in a more general consideration a ReRAM cell that obeys the empirical SET law should exhibit highly nonlinear switching kinetics. In this case the driving force for resistance change during the current compliance is reduced tremendously and the LRS resistance can be precisely tuned. This behavior is independent of the origin of the switching kinetics of a particular ReRAM, *e.g.* electric field, voltage or temperature.

RESET

To analyze the empirical relationship between the RESET current and SET current an expression for the RESET current has to be derived. Since the RESET current is defined as the peak current during the RESET process, this means $\mathrm{d}I/\mathrm{d}t = 0$. As a simplification it is assumed that the RESET event occurs before the peak voltage is reached. Hence, the RESET current is given by eqn (4), where x is given by eqn (5). The current equation can be further simplified by setting the term $1/x$ to a constant value $1/x_{\mathrm{ON}}$. This approximation is valid since the exponential dependence of the tunnelling current on x dominates. With these approximations the current now reads

$$I \approx -\frac{3}{2}C\sqrt{2m_{\mathrm{eff}}\Delta W_0}\,\frac{e^2}{h^2}\frac{1}{x_{\mathrm{ON}}} \times \exp\left(-\frac{4\pi}{h}x\sqrt{2m_{\mathrm{eff}}\Delta W_0}\right)A_{\mathrm{fil}}\beta(t-T_0) \quad (19)$$

Differentiating eqn (19) with respect to t, setting to zero and solving for t_{peak} with the help of the Lambert-W function yields

$$t_{\mathrm{peak}} = T_0 + \frac{k_{\mathrm{B}}T}{ze\alpha(1-\alpha)\beta}W\left(\frac{\alpha(1-\alpha)\beta\frac{ze}{k_{\mathrm{B}}T}}{\frac{4\pi}{h}\sqrt{2m_{\mathrm{eff}}\Delta W_0}\,\frac{M_{\mathrm{Me}}}{ze\rho_{\mathrm{m,Me}}}j_0\left(\frac{A_{\mathrm{ac}}}{A_{\mathrm{fil}}}\right)^{1-\alpha}}\right) \quad (20)$$

The RESET voltage can now be calculated according to $V_{\mathrm{RESET}} = -\beta(t_{\mathrm{peak}} - T_0)$ as

$$V_{\mathrm{RESET}} = -\frac{k_{\mathrm{B}}T}{ze\alpha(1-\alpha)}W\left(\frac{\alpha(1-\alpha)\beta\frac{ze}{k_{\mathrm{B}}T}}{\frac{4\pi}{h}\sqrt{2m_{\mathrm{eff}}\Delta W_0}\,\frac{M_{\mathrm{Me}}}{ze\rho_{\mathrm{m,Me}}}j_0\left(\frac{A_{\mathrm{ac}}}{A_{\mathrm{fil}}}\right)^{1-\alpha}}\right) \quad (21)$$

Note that the derived equation for the RESET voltage (21) is independent of the previous state of the ECM cell and depends only on the material parameters and the sweep rate. Thus, under the same sweeping conditions the RESET voltage is constant for a particular ECM cell. By inserting eqn (21) into eqn (16)

$$x_{\mathrm{RESET}} = x_{\mathrm{ON}} + \frac{M_{\mathrm{Me}}}{ze\rho_{\mathrm{m,Me}}}j_0\left(\frac{A_{\mathrm{ac}}}{A_{\mathrm{fil}}}\right)^{1-\alpha}\frac{k_{\mathrm{B}}T}{ze\alpha(1-\alpha)\beta} \times\left(\exp\left(W\left(\frac{\alpha(1-\alpha)\beta\frac{ze}{k_{\mathrm{B}}T}}{\frac{4\pi}{h}\sqrt{2m_{\mathrm{eff}}\Delta W_0}\,\frac{M_{\mathrm{Me}}}{ze\rho_{\mathrm{m,Me}}}j_0\left(\frac{A_{\mathrm{ac}}}{A_{\mathrm{fil}}}\right)^{1-\alpha}}\right)\right)-1\right) \quad (22)$$

results, where the -1 term will be neglected in the following. This equation can be rewritten using the identity $\exp(W(b)) = b/W(b)$ (ref. 33) so that

$$x_{\mathrm{RESET}} = x_{\mathrm{ON}} + \frac{h}{4\pi\sqrt{2m_{\mathrm{eff}}\Delta W_0}}W^{-1} \times\left(\frac{\alpha(1-\alpha)\beta\frac{ze}{k_{\mathrm{B}}T}}{\frac{4\pi}{h}\sqrt{2m_{\mathrm{eff}}\Delta W_0}\,\frac{M_{\mathrm{Me}}}{ze\rho_{\mathrm{m,Me}}}j_0\left(\frac{A_{\mathrm{ac}}}{A_{\mathrm{fil}}}\right)^{1-\alpha}}\right) \quad (23)$$

The RESET current can now be calculated using eqn (23), (19) and $G_{\mathrm{ON}} = I_{\mathrm{cc}}/V_{\mathrm{ON}}$ as

$$I_{\mathrm{RESET}} = \frac{V_{\mathrm{RESET}}}{V_{\mathrm{ON}}} \times\exp\left(-W^{-1}\left(\frac{\alpha(1-\alpha)\beta\frac{ze}{k_{\mathrm{B}}T}}{\frac{4\pi}{h}\sqrt{2m_{\mathrm{eff}}\Delta W_0}\,\frac{M_{\mathrm{Me}}}{ze\rho_{\mathrm{m,Me}}}j_0\left(\frac{A_{\mathrm{ac}}}{A_{\mathrm{fil}}}\right)^{1-\alpha}}\right)\right)I_{\mathrm{SET}} \quad (24)$$

Hence, the linear dependence of the RESET current on the SET current is mathematically derived. Fig. 4(a) shows the

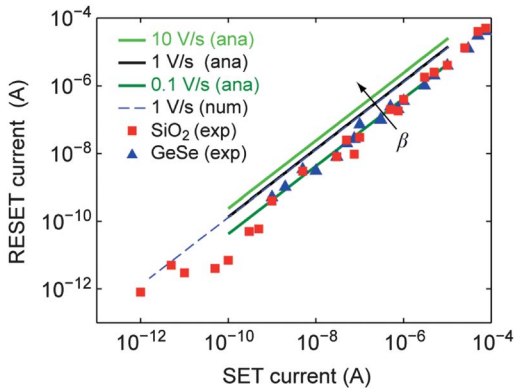

Fig. 4 Calculated RESET *vs.* SET current using the analytical model for sweep rates $\beta = 0.1$ V s^{-1} (dark green), 1 V s^{-1} (black), and 10 V s^{-1} (light green). For comparison the analytical data for a Cu/SiO_2 based ECM cell and a Ag/GeSe based ECM cell are shown as red squares and blue triangles, respectively. Here, only a subset of the experimental data comparable to the simulation range is shown.[9] The simulation result obtained using the numerical model[5] is illustrated as a dashed blue line.

calculated RESET currents *vs.* SET currents using eqn (24) for three different sweep rates β illustrating the linear dependency compared to the numerical simulation results[5] and the experimental data. Apparently, the analytical and the numerical solutions coincide and the experimentally observed trend is reproduced. The experimental data, however, exhibits a lower RESET current as predicted by the model as discussed in the *I–V* characteristics section. The influence of the sweep rate on the RESET current is also illustrated in Fig. 4(a): the higher the sweep rate, the higher the RESET current. This result follows directly from eqn (24). The RESET current, which depends linearly on the voltage, increases due to the increase in RESET voltage for increasing sweep rates as illustrated in Fig. 4(b). Based on the above considerations the origin of the empirical law $I_{RESET} = AI_{SET}$ can be identified to (i) the linear *I–V* characteristics and (ii) the highly nonlinear switching characteristics resulting in a RESET voltage that is independent of the previous LRS. Both conditions were also met in the variable diameter model of Ielmini[13] and thus can be considered universal. The physical origin of the linear LRS is not relevant. It can be for example ohmic conduction[13] or direct tunnelling as in the present model. Also a nonlinear *I–V* might lead to the generic RESET characteristics. But for this the current asymmetry of the positive and negative voltage branch should be independent of the resistance state. If the asymmetry of the positive and negative voltage changes with the set resistance state, a linear dependence of the RESET current on the SET current would not be achieved.

Conclusions

In summary, we presented an analytic model for the resistive switching in ECM cells that can be easily introduced into circuit simulators. The model is valid as long as the switching kinetics are electron-transfer limited and $|V| \gg k_B T/ze$. Both conditions are typically fulfilled for fast pulse operation. Using the model an analytical equation for the RESET current is derived. Based on the analytical analyses the origin of the generic SET and RESET characteristics in ECM cells can be identified:

(1) The origin of the empirical law $R_{LRS} \propto I_{SET}^{-1}$ in ECM cells is demonstrated to be the nonlinear switching kinetics due to the electron transfer reaction at the boundaries and the exponential gap dependence of the tunneling voltage. This combination results in a double-exponential decrease of the driving force for filamentary growth during current control.

(2) For ReRAM cells in general the empirical law $R_{LRS} \propto I_{SET}^{-1}$ has its origin in the highly nonlinear switching kinetics that leads to a huge decrease of the driving force of resistance change under current control. In this case the physical origin of the switching kinetics is irrelevant. It is also independent of the physical representation of the LRS state, *e.g.* variable gap or variable diameter mode.

(3) The relationship $I_{RESET} \propto I_{SET}$ of ECM cells results from the strongly nonlinear switching kinetics, which results in a virtually constant RESET voltage, and the linear *I–V* relationship of the LRS state. All ReRAMs that fulfill these two conditions also obey the empirical RESET law.

(4) The empirical RESET law might also apply to ReRAMs with a nonlinear *I–V* relationship if the current asymmetry in the positive and negative voltage branch is independent of the programmed resistance state. If the current asymmetry depends on the resistance state, the ReRAM cell would not obey the empirical RESET law.

Acknowledgements

This work has been supported in parts by the Deutsche Forschungsgemeinschaft (SFB 917).

Notes and references

1 ITRS, *The International Technology Roadmap for Semiconductors*, ITRS, 2011 edn, 2011.
2 J. J. Yang, D. B. Strukov and D. R. Stewart, *Nat. Nanotechnol.*, 2013, **8**, 13.
3 R. Waser, R. Dittmann, G. Staikov and K. Szot, *Adv. Mater*, 2009, **21**, 2632.
4 I. Valov, R. Waser, J. R. Jameson and M. N. Kozicki, *Nanotechnology*, 2011, **22**, 254003.
5 S. Menzel, U. Böttger and R. Waser, *J. Appl. Phys.*, 2012, **111**, 014501.
6 D. Ielmini, R. Bruchhaus and R. Waser, *Phase Transitions*, 2011, **84**, 570.
7 R. Waser, S. Menzel and R. Bruchhaus, *Nanolectronics and Information Technology*, Wiley-VCH, 3rd edn, ch. 30, 2012.
8 Y. Bernard, V. T. Renard, P. Gonon and V. Jousseaume, *Microelectron. Eng.*, 2011, **88**, 814.
9 C. Schindler, PhD thesis, RWTH Aachen, 2009.
10 S. Tappertzhofen, I. Valov and R. Waser, *Nanotechnology*, 2012, **23**, 145703.
11 K. Tsunoda, Y. Fukuzumi, J. R. Jameson, Z. Wang, P. B. Griffin and Y. Nishi, *Appl. Phys. Lett.*, 2007, **90**, 113501.

12 N. Derhacobian, S. C. Hollmer, N. Gilbert and M. N. Kozicki, *Proc. IEEE*, 2010, **98**, 283.
13 D. Ielmini, *IEEE Trans. Electron Devices*, 2011, **58**, 4309.
14 E. Scheer, N. Agrait, J. Cuevas, A. Yeyati, B. Ludoph, A. Martin-Rodero, G. Bollinger, J. van Ruitenbeek and C. Urbina, *Nature*, 1998, **394**, 154.
15 K. Terabe, T. Hasegawa, T. Nakayama and M. Aono, *Nature*, 2005, **433**, 47.
16 S. Choi, S. Balatti, F. Nardi and D. Ielmini, *IEEE Electron Device Lett.*, 2012, **33**, 1189.
17 T. Tsuruoka, K. Terabe, T. Hasegawa and M. Aono, *Nanotechnology*, 2010, **21**, 425205.
18 W. Guan, S. Long, Q. Liu, M. Liu and W. Wang, *IEEE Electron Device Lett.*, 2008, **29**, 434.
19 C. Schindler, S. C. P. Thermadam, R. Waser and M. N. Kozicki, *IEEE Trans. Electron Devices*, 2007, **54**, 2762.
20 S. Menzel, N. Adler, J. van den Hurk, S. Tappertzhofen, I. Valov and R. Waser, *5th IEEE International Memory Workshop (IMW)*, 2013, p. 4.
21 N. Raghavan, R. Degraeve, L. Goux, A. Fantini, D. J. Wouters, G. Groeseneken and M. Jurczak, *Proceedings of the 2013 Symposium on VLSI Technology*, 2013.
22 I. Valov and M. N. Kozicki, *J. Phys. D: Appl. Phys.*, 2013, **46**, 074005.
23 I. Valov, E. Linn, S. Tappertzhofen, S. Schmelzer, J. v. d. Hurk, F. Lentz and R. Waser, *Nat. Commun.*, 2013, **4**, 1771.
24 U. Russo, D. Kamalanathan, D. Ielmini, A. L. Lacaita and M. N. Kozicki, *IEEE Trans. Electron Devices*, 2009, **56**, 1040.
25 S. Menzel, B. Klopstra, C. Kügeler, U. Böttger, G. Staikov and R. Waser, *Mater. Res. Soc. Symp. Proc.*, 2009, **1160**, 101.
26 S. Yu and H.-S. Wong, *IEEE Trans. Electron Devices*, 2011, **58**, 1352.
27 D. B. Strukov and R. S. Williams, *Appl. Phys. A: Mater. Sci. Process.*, 2011, **102**, 851.
28 D. Ielmini, F. Nardi and C. Cagli, *Nanotechnology*, 2011, **22**, 254022.
29 M. Faraday, *Philos. Trans. R. Soc. London*, 1834, **124**, 77.
30 C. H. Hamann, A. Hamnett and W. Vielstich, *Electrochemistry*, Wiley-VCH, Weinheim, 2007.
31 J. G. Simmons, *J. Appl. Phys.*, 1963, **34**, 1793.
32 S. Menzel, S. Tappertzhofen, R. Waser and I. Valov, *Phys. Chem. Chem. Phys.*, 2013, **15**, 6945.
33 R. Corless, G. Gonnet, D. Hare, D. Jeffrey and D. Knuth, *Adv. Comput. Math.*, 1996, **5**, 329.
34 S. Tappertzhofen, S. Menzel, I. Valov and R. Waser, *Appl. Phys. Lett.*, 2011, **99**, 203103.

